

A state estimate of the routes of the upper branch of the Atlantic Meridional Overturning Circulation

Louise Rousselet¹, Paola Cessi², and Gaël Forget³

¹Scripps Institution of Oceanography, University of California, San Diego

²Scripps Institution of Oceanography, University of California, San Diego

³Massachusetts Institute of Technology

November 21, 2022

Abstract

The origins of the upper branch of the Atlantic Meridional Overturning Circulation (AMOC) are traced with backward-in-time Lagrangian trajectories, quantifying the partition of volume transport between different routes of entry from the Indo-Pacific sector into the Atlantic. Particles are advected by a three-dimensional, incompressible velocity field from a recent release of “Estimating the Circulation and Climate of the Ocean’ (ECCOV4). This time-variable velocity field is a dynamically consistent interpolation of over one billion oceanographic observations collected between 1992 and 2015. Of the 13.6 Sverdrups ($1\text{Sv} = 10^6 \text{ m}^3/\text{s}$) of upper and intermediate water flowing northward across 6°S , 15% enters the Atlantic from Drake Passage, 35% enters from the straits between Asia and Australia, termed the Indonesian Throughflow, and 49% comes from the region south of Australia, termed the Tasman Leakage. The salinity budget shows that the AMOC exports freshwater out of the Atlantic.

1 **A state estimate of the routes of the upper branch of the Atlantic**
2 **Meridional Overturning Circulation**

3 **Louise Rousselet¹, Paola Cessi^{1*}, Gael Forget²**

4 ¹Scripps Institution of Oceanography, University of California, San Diego, USA

5 ²Dept. of Earth, Atmospheric and Planetary Sciences, Massachusetts Institute of Technology, Cambridge, MA, USA

6 **Key Points:**

- 7 • The upper limb of the meridional overturning circulation originates primarily from the
8 Tasman Leakage and the Indonesian Throughflow
9 • 97% of the upper limb of the meridional overturning circulation enters the Atlantic from
10 the Agulhas region, around the tip of South Africa
11 • Because its upper limb is saltier than its lower limb, the overturning exports freshwa-
12 ter out of the Atlantic basin.

*Paola Cessi, Scripps Institution of Oceanography,
University of California, San Diego,
La Jolla, CA 92039-0213, USA

Corresponding author: Paola Cessi, pcessi@ucsd.edu

Abstract

The origins of the upper branch of the Atlantic Meridional Overturning Circulation (AMOC) are traced with backward-in-time Lagrangian trajectories, quantifying the partition of volume transport between different routes of entry from the Indo-Pacific sector into the Atlantic. Particles are advected by a three-dimensional, incompressible velocity field from a recent release of “Estimating the Circulation and Climate of the Ocean” (ECCOv4). This global time-variable velocity field is a dynamically consistent interpolation of over one billion oceanographic observations collected between 1992 and 2015. Of the 13.6 Sverdrups ($1\text{ Sv} = 10^6 \text{ m}^3/\text{s}$) of upper and intermediate water flowing northward across 6°S , 15% enters the Atlantic from Drake Passage, 35% enters from the straits between Asia and Australia, termed the Indonesian Through-flow, and 49% comes from the region south of Australia, termed the Tasman Leakage. The salinity budget shows that the AMOC exports freshwater out of the Atlantic.

Plain Language Summary

Particle trajectories in the upper limb of the Atlantic Meridional Overturning Circulation (AMOC) are traced from the equatorial Atlantic to different sections of origin in the Southern Ocean. The three-dimensional velocity moving the particles is an estimate combining over a billion of observations with a global ocean model that conserves mass, momentum, temperature, salinity and sea-ice over a regular grid. 97% of the particles enter the Atlantic from the tip of South Africa, as a relatively warm and salty water mass, while the remaining 3% enters from the tip of South America cold and fresh. Because the upper limb of the AMOC entering the Atlantic is saltier than the exiting lower limb, this estimate shows that the AMOC might collapse given appropriate freshwater perturbations.

1 Introduction

The meridional overturning circulation (MOC) of the Ocean is a key component of Earth’s climate system. The Atlantic-sector MOC transports heat northwards at all latitudes (Hsiung, 1985), modulating the position of the Inter Tropical Convergence Zone (Kang et al., 2008).

The MOC includes northward flow of intermediate and upper waters from the Southern Ocean into the Atlantic, which are eventually transformed into North Atlantic Deep Water (NADW) in the Labrador and Nordic Seas. NADW then flows southward at depth upwelling in the Southern Ocean to close the *mid-depth cell* (red contours in figure 1). An equivalent mid-depth cell is absent in the Indo-Pacific sector (Cessi, 2019).

Water that has upwelled from the lower, southward branch of the mid-depth cell in the Indo-Pacific sector (south of 30°S) can return to the North Atlantic through two pathways: the *warm route*, i.e. *westward and northward around the tip of South Africa* (Gordon, 1986), or the *cold route*, i.e. *eastward and northward around Drake Passage* (Rintoul, 1991). The quantitative contributions of these two routes differ among estimates, but this partition is important for the transport of heat and freshwater into the Atlantic. Water that enters the South Atlantic through the warm route is warm and salty, while that entering through the cold route is fresh and cold. Many model simulations have shown that if the cold route prevails, the MOC is robust to freshwater perturbation in the high latitudes of the North Atlantic and Arctic. Vice versa, if the exchange is mostly via the warm route, then North Atlantic freshwater perturbations shut down the MOC (de Vries & Weber, 2005; Beal et al., 2011; Drijfhout et al., 2011).

Several observational and numerical studies have estimated the relative contribution of the two routes. Most observational studies support the cold water route (Schmitz Jr, 1995; Macdonald, 1998; Sloyan & Rintoul, 2001; Talley, 2013), while most numerical studies and one observational analysis favor the warm water route (Speich et al., 2001; Holfort & Siedler, 2001; Donners & Drijfhout, 2004; Speich et al., 2007; Rodrigues et al., 2010; Cessi & Jones, 2017; Ruhs et al., 2019). Donners and Drijfhout (2004) illustrate the difficulty of establishing the

61 origin of the MOC’s upper branch using inverse models with sparse observations at hydrographic
 62 sections: this method applied to the output of an eddy-resolving computation leads to a qual-
 63 itatively different partition between routes than that obtained with Lagrangian analysis.

64 A major difficulty with identifying routes of the upper branch of the MOC is that inter-
 65 basin connection is mediated by currents in the Southern Ocean, which are dominated by a
 66 recirculating component associated with the Antarctic Circumpolar Current (ACC) (Forget &
 67 Ferreira, 2019). The ACC recirculates about 50 Sv (1 Sv = 10^6 m³/s) in the top 1000 meters
 68 of the water column, while the upper branch of the MOC carries about 14Sv, a small fraction
 69 of the recirculating transport (Cessi, 2019).

70 To overcome this difficulty, we quantify the pathways of intermediate water from the Indo-
 71 Pacific to the Atlantic using Lagrangian analysis. The method consists of tracking particle tra-
 72 jectories backwards in time from an “exit” section in the South Atlantic (here 6°S) to specific
 73 “entry” sections. The origin of particle trajectories is identified by the backward-in-time first
 74 passage through one of the “entry” sections. The quantification of mass transport with parti-
 75 cle trajectories is performed by initially populating the exit section with a large number of par-
 76 ticles whose concentration is proportional to the local transport. Each particle carries a small
 77 amount of transport that is conserved following the trajectory because the velocity vector field
 78 conserves mass (volume). This type of calculations has been successfully performed using ve-
 79 locity fields from ocean general circulation models (Döös, 1995; Speich et al., 2001; Rühls et
 80 al., 2019), but not with global observations. To estimate Lagrangian transport, it is necessary
 81 to have velocities interpolated over a global grid, tightly constrained by observations, while
 82 strictly conserving mass. A product that satisfies these requirements is the three-dimensional,
 83 time-variable, incompressible velocity from “Estimating the Circulation and Climate of the Ocean”
 84 (ECCOV4) (Forget, Campin, et al., 2015; Fukumori et al., 2017).

85 The modern measure of the MOC is given in terms of the “residual” transport within
 86 isopycnal layers, rather than depth layers. The residual overturning circulation measures the
 87 (potential) density transport, rather than the volume transport: it is more meaningfully asso-
 88 ciated with the transport of tracers than is the overturning in depth coordinates (Young, 2012).
 89 Specifically, the residual overturning circulation captures the transport effected not only by the
 90 average meridional velocity but also by waves, eddies, and gyres with zero time- or zonally
 91 averaged velocity.

92 In models that do not fully resolve mesoscale processes, the eddy-flux of tracers needs
 93 to be parametrized. The parametrized eddy-transport is typically expressed in terms of isopyc-
 94 nal diffusion and a “bolus” velocity related to the slope of isopycnals (Redi, 1982; Gent &
 95 McWilliams, 1990; Griffies, 1998). In these models the appropriate way to calculate the resid-
 96 ual transport of the MOC is to use the sum of Eulerian velocity plus the bolus velocity, in-
 97 tegrated over density layers rather than depth layers. In figure 1, the time-averaged and lon-
 98 gitudinally integrated MOC is calculated in density coordinates and latitude, using σ_2 , i.e. po-
 99 tential density referred to 2000 decibars, as the vertical coordinate. Accordingly, the veloc-
 100 ity used to calculate Lagrangian trajectories is the sum of Eulerian velocity plus the bolus ve-
 101 locity in all three dimensions.

102 2 Calculation of Lagrangian trajectories

103 The velocities used in the calculation of Lagrangian trajectories are the monthly clima-
 104 tology available in the release 3 of ECCOV4 on the native model grid at 1° horizontal res-
 105 olution (the *Lat-Lon-Cap-90* grid as defined in Forget, Campin, et al. (2015)) and with 50 ver-
 106 tical levels (Forget, Campin, et al., 2015; Fukumori et al., 2017). These velocities derive from
 107 the dynamically-consistent assimilation of over one billion observations for the period 1992-
 108 2015 into a primitive-equations ocean-sea-ice model that satisfies exact conservation laws for
 109 mass, temperature, salinity and sea-ice.

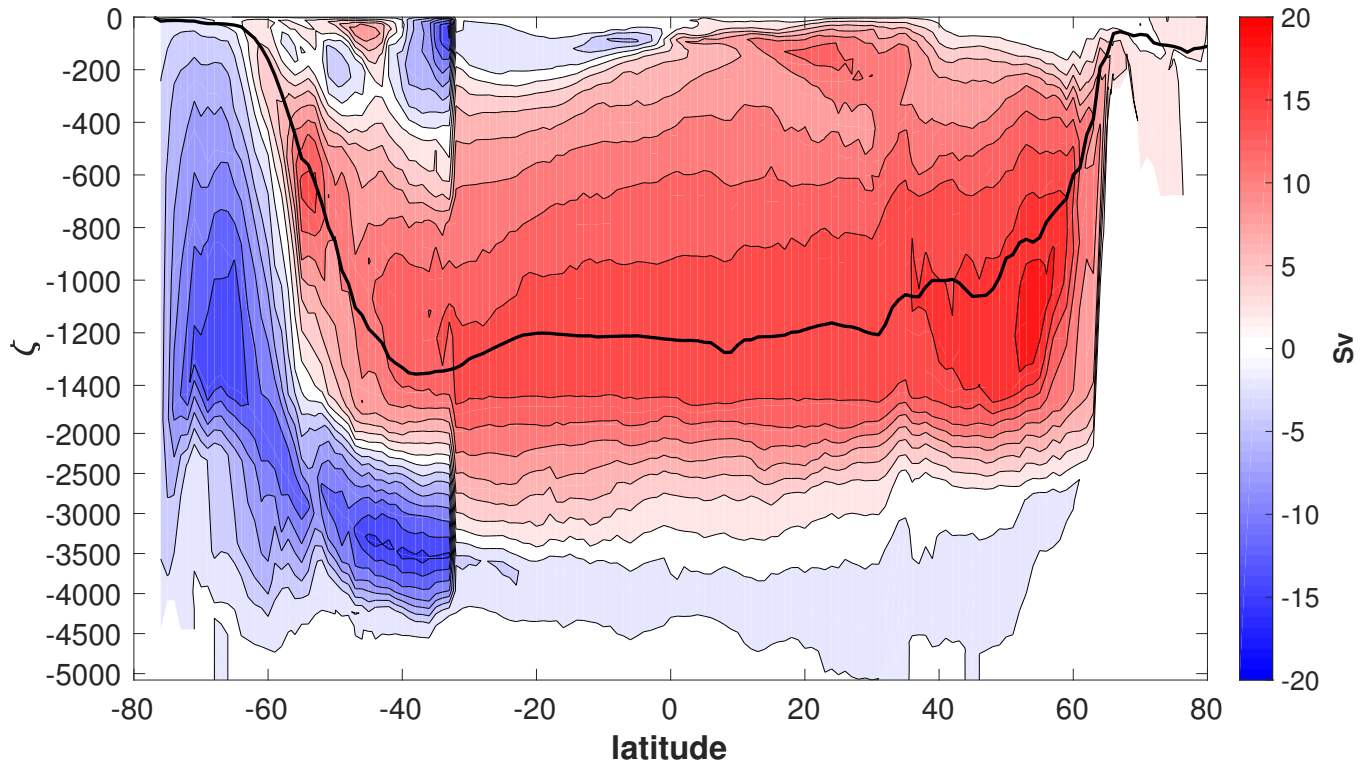


Figure 1. Residual meridional overturning circulation vertically integrated above surfaces of constant σ_2 , then time averaged and zonally integrated in the Southern Ocean south of 37°S , and in the Atlantic sector north of 37°S , as a function of latitude (abscissa) and σ_2 (ordinate). The ordinate is remapped into a depth-like coordinate ζ (latitude, σ_2) which represents the time and zonal averaged (over all longitudes) depth of each σ_2 surface. The ECCO4 (release 3) horizontal velocity (Eulerian+bolus), temperature and salinity re-analysis fields are used. Positive values (red) indicate clockwise circulation. The contour interval is 2 Sv (1 Sv = 10^6 m³/s). The thick black line marks the depth ζ (latitude, $\sigma_2=36.6\text{ kg/m}^3$), which approximately divides the upper and lower branches of the residual MOC.

110 The assimilated data consist of satellite products (including along-track altimetry, mean
 111 dynamic topography, remotely sensed ocean bottom pressure, sea-surface temperature, sea-ice
 112 concentration and surface salinity), and temperature and salinity profiles collected in-situ (in-
 113 cluding from all Argo floats). To minimize misfit between the model and the observations, the
 114 following model parameters are optimized (Forget, Campin, et al., 2015; Fukumori et al., 2017):
 115 initial conditions in January 1992, air-sea interactions throughout 1992-2015, diapycnal and
 116 isopycnal tracer diffusion rates, and the parameterized advective effect of mesoscale eddies (Gent
 117 & McWilliams, 1990; Forget, Ferreira, & Liang, 2015). Because the optimization uses the ad-
 118 joint and forward versions of the model, for fifty iterations, the adjustment of the control pa-
 119 rameters can be effected and beneficial on a time-scale of hundreds of years, even though the
 120 data record is only 24 years long (Forget, Ferreira, & Liang, 2015).

121 Many studies have looked at various measures and methods to assess the ECCOv4 es-
 122 timate, which collectively affirm its value for understanding both the Ocean climatology and
 123 its variability from observations (Forget, Campin, et al., 2015; Fukumori et al., 2017; Forget
 124 & Ponte, 2015; Forget & Ferreira, 2019; Jackson et al., 2019). The estimate of the MOC ac-
 125 cording to ECCOv4 is in broad agreement with several independent (i.e. not assimilated) es-
 126 timates [see Table 1 in Cessi (2019)]. The ACC transport at Drake Passage in ECCOv4 is 155
 127 Sv which is intermediate between the two recent independent ‘in-situ’ estimates of Cunningham

128 et al. (2003) (134 ± 11 Sv) and Donohue et al. (2016) (173 ± 11 Sv), and in the middle of the
 129 estimates compiled by Uotila et al. (2019).

130 To determine the Lagrangian trajectories, the ECCOv4 climatological monthly veloci-
 131 ties are interpolated in space using an incompressibility-preserving, transport-weighted algo-
 132 rithm (Döös, 1995; Blanke & Raynaud, 1997) and advected backward in time using a Runge-
 133 Kutta fourth-order scheme for 2011 years (more details in the supplemental material). Because
 134 the climatological monthly velocities are one-year periodic, the annual cycle can be repeated
 135 as many times as needed. Particles are initialized every month for one year (for a total of 63482
 136 particles) at 6°S in the South Atlantic, at depths above the $\sigma_2 = 36.6\text{kg/m}^3$ surface: this de-
 137 fines the “exit section”. The $\sigma_2 = 36.6\text{kg/m}^3$ surface marks the lower boundary of the upper,
 138 northward branch of the MOC. Each particle carries about 2×10^{-4} Sv so that the number
 139 of particles per each grid-face on the section is proportional to the transport of that grid-face
 140 (the exact transport of each particle is recorded). Because the three-dimensional velocity vec-
 141 tor is exactly incompressible, the transport of each particle is conserved following the trajec-
 142 tory (Döös, 1995; Blanke & Raynaud, 1997). This conservation can be used to quantify the
 143 transport through different “entry” sections, determining the origin of waters that feed the up-
 144 per branch of the MOC. The place and time of origin is defined as being the first passage from
 145 the exit to one of the four entry sections going backward in time.

146 The entry sections at which we measure the first-passage are at Drake Passage (DP, at
 147 66°W), at the Indonesian Throughflow (IT, at 116°E), at the Tasman leakage region (TL, at
 148 116°E) and in the South Atlantic at 6°S for depths below the $\sigma_2 = 36.6\text{kg/m}^3$ surface, i.e.
 149 in the lower limb of the MOC (cf. figure 2). The northward transport at the “exit” section is
 150 13.64 Sv. The particles are followed backward in time for 2011 years, after which all but 0.3%
 151 have moved through one of the entry sections. The region encompassed by the entry and exit
 152 sections has a net evaporation of 0.44Sv, but our procedure does not allow particles to exit or
 153 enter the air-sea boundary: instead particles that try to escape the surface are reinjected into
 154 the first model level. The computation was repeated for 512 years with double the number of
 155 particles (126964), and the transport values at the exit region differ at most by 0.2% over that
 156 time from those with 63482 particles. Henceforth, we present the result with 63482 particles,
 157 which we trust to be robust. By convention, the particle trajectories and their transport are de-
 158 scribed as forward-in-time in the following sections.

159 3 Routes of the upper limb of the MOC

160 The MOC upper limb pathways are quantified by considering the subsets of trajectories
 161 connecting the exit section (6°S) with each of the entry sections. Figure 2 shows the trans-
 162 port streamfunction (contours) obtained by summing vertically the particles in bins of $1^\circ \times$
 163 1° , weighted by their transport (magnitude and sign). The sign convention for the transport
 164 streamfunction is for forward-in-time trajectories. The color shading shows the depth of the
 165 $\sigma_2 = 36.6\text{kg/m}^3$ surface, averaged over the 24-years period covered by ECCOv4. The trans-
 166 port streamfunction flows around the edge of the Southern Ocean supergyre, whose shape is
 167 highlighted by the depth contours of the $\sigma_2 = 36.6\text{kg/m}^3$ (Speich et al., 2001, 2002, 2007).
 168 All trajectories converge to the region separating the subtropical and tropical gyres in the South
 169 Atlantic before reaching 6°S . The net transport at the exit section is composed of:

- 170 **DP** 2.0 Sv across Drake Passage at 66°W ;
- 171 **IT** 4.8 Sv across the Indonesian Throughflow at 116°E ;
- 172 **TL** 6.6 Sv at 130°E , south of Australia (Tasman Leakage);
- 173 **6°S** 0.2 Sv at 6°S flowing southward at depths below the $\sigma_2 = 36.6\text{kg/m}^3$ surface.

174 Trajectories that enter through DP flow around the edge of the subtropical gyres of the
 175 South Atlantic and of the South Indian Ocean before moving northward across the exit sec-
 176 tion at 6°S , so that a large fraction of the particles entering DP (80% or 1.6 Sv) subsequently
 177 go through the Agulhas current region at the tip of South Africa. This pathway has been termed

178 the “indirect cold route” (Gordon et al., 1992) and has a typical transit time longer than 25
 179 years, shown by the secondary peaks in the distribution on the bottom panel of figure 3. The
 180 direct cold route, which avoids the Agulhas Current, is a small fraction (20% or 0.4Sv), with
 181 typical transit times of 12 years.

182 Most trajectories come through the Tasman Leakage and the Indonesian throughflow, all
 183 steered by the flow around the outer edge of the supergyre. Interestingly, the TL entry sec-
 184 tion carries more transport (6.6Sv) than the IT (4.8Sv), while the opposite is true in previous
 185 analyses (Speich et al., 2001). Our estimate of the median transit time (see figure 3) is 30 years
 186 for DP and IT, and 33 years for TL. Both median transit times are substantially shorter than
 187 those of Speich et al. (2001), who found 52 years for DP and IT, and 81 years for TL. Fur-
 188 thermore, the e-folding time of the transit-time distribution across TL is shorter (30 years) than
 189 the e-folding time across IT (47 years). In all cases, there are long tails in the transit-time dis-
 190 tributions, indicating extensive recirculations.

191 The total transport entering the South Atlantic from the east at 22°E (the tip of South
 192 Africa) carries 97% of the transport, while DP through the direct cold route only carries 3%
 193 of the MOC. These results should be compared with the partition found in the analysis of an
 194 eddy-resolving simulation (Rühs et al., 2019), which finds a 60-40% split between these two
 195 routes, i.e. ten times what we find for the direct cold route. One reason for this difference is
 196 that ECCOv4 has a stronger climatological eastward transport of the Antarctic Circumpolar
 197 Current at Drake passage (155 Sv) than the eddy-resolving, non-assimilative model simula-
 198 tion of Rühs et al. (2019) (116 Sv) – allowing ECCOv4 to carry trajectories that cross DP away
 199 from the South Atlantic more efficiently, and perhaps more realistically.

200 **4 Thermodynamic properties of the upper limb of the MOC**

201 The thermodynamic characteristics at the entry regions differ markedly between DP, IT
 202 and TL. The right panels in figure 4 show the potential temperature-salinity ($\theta - S$) volumet-
 203 ric diagram (colored points, weighted by transport), for the particles at three entry regions, plus
 204 at the Agulhas section at 22°E (boxed inset in bottom right panel). The water at DP is cold
 205 (mean temperature = 2.3°C) and fresh (mean salinity = 34.3 PSU); the water at the IT is
 206 warm (mean temperature = 17.2°) and slightly saltier (mean salinity = 34.4 PSU); the wa-
 207 ter at TL is intermediate in temperature between DP and IT (mean temperature = 8.7°C) and
 208 saltier (mean salinity = 34.6 PSU). The TL water includes a fraction which shares the prop-
 209 erties originating at the Drake Passage, i.e. cold and relatively fresh: this water is associated
 210 with the outer streamlines (positive near zero values), which flow eastward in the southern re-
 211 gion of the ACC and then turn around to enter the TL section.

212 As in the original “warm-cold route” nomenclature (Gordon, 1986), there is a substan-
 213 tial difference in temperature between the waters originating in DP and those originating in
 214 IT and TL, while the distinction in salinity is not as pronounced. However, by the time the
 215 particles reach 6°S the differences between these characteristics are erased and the three groups
 216 are undistinguishable in $\theta - S$ space, as found in Rühs et al. (2019). This is because all tra-
 217 jectories eventually merge into the narrow South Equatorial Current and North Brazil Current
 218 before reaching 6°S. This merger facilitates property transformations along isopycnals. Prop-
 219 erties are also transformed through diapycnal mixing and air-sea interaction across isopycnals.
 220 Furthermore, the IT, TL and “indirect-route” DP waters are all eventually squeezed into the
 221 narrow Agulhas Current system, from which they emerge as a single water mass in the South
 222 Atlantic, with a tight $\theta - S$ relation at 22°E (the boxed inset in the bottom right panel of fig-
 223 ure 4), with an average salinity of 35 PSU.

224 The bulk of particles arriving at 6°S have a salinity near 35.6 PSU which is larger than
 225 any of the water masses at their sections of origin, or at 22°E. This requires loss of freshwa-
 226 ter in the journey to and across the South Atlantic in this region that loses a total of 0.44 Sv
 227 of freshwater at the surface. The net surface evaporation is consistent with an increase in La-

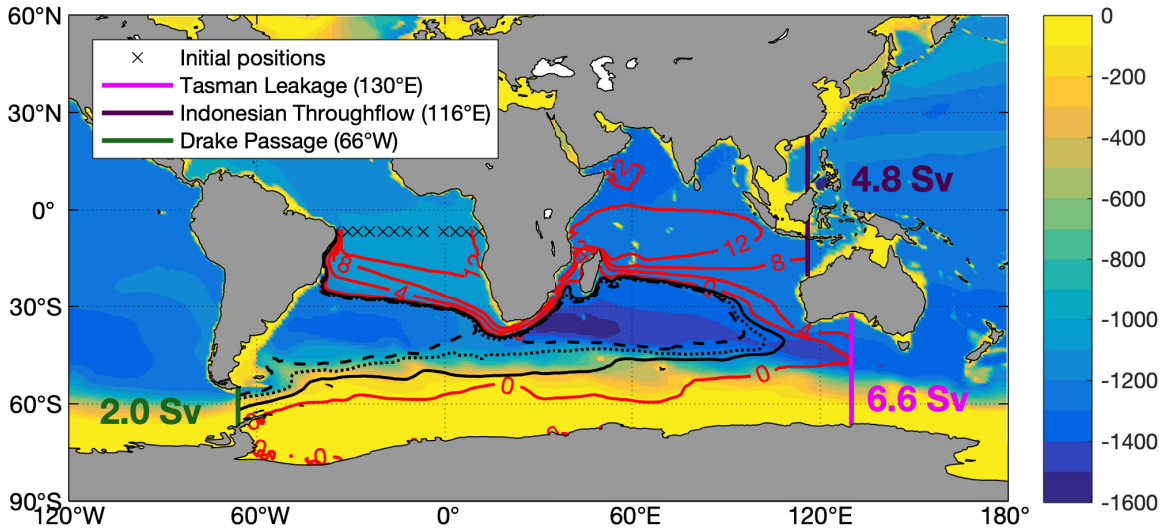


Figure 2. Transport streamfunction calculated from particle trajectories (contours): red contours are 4Sv apart; the black solid contour is -1Sv, the black dotted contour is -1.5Sv and the black dashed contour is -1.75Sv. The color shading shows the depth (in m) of the time-averaged $\sigma_2=36.6\text{ kg/m}^3$. The exit section at 6°S is marked by black x, and the entry sections are at Drake passage (66°W green), at Tasman Leakage (130°E magenta), and Indonesian Throughflow (116°E dark purple). The transport at each entry section is marked in the corresponding color. The transport at the exit section is 13.6Sv. After 2011 years there are 0.04Sv still recirculating in the region bounded by the four sections, and 0.2Sv have entered 6°S from the North below $\sigma_2=36.6\text{ kg/m}^3$.

228 grangian transport of salinity between the entry and exit regions of 16.6 PSU Sv, which is equiv-
 229 alent to a mass evaporation of 0.46 Sv at an average surface salinity of 36 PSU.

230 While the particles become saltier from their region of origin at DP, IT and TL, the par-
 231 ticles from DP and TL become sufficiently warmer to overcome the density increase due to
 232 salinification. The net result is that, with the exception of the particles originating in the IT,
 233 the particles at 6°S become less dense than at their origin. The particles originating at the IT
 234 experience a general cooling as they pass through the Agulhas Current system, only to be warmed
 235 up again in the South Atlantic. Typical trajectories from the entry regions of TL, IT, DP (in-
 236 cluding both direct and indirect route) to the exit region are shown in the supplemental ma-
 237 terial. The animations provide a visualization of both time scales and pathways, while also re-
 238 vealing salinity and potential temperature transformations along the trajectories.

239 The particles entering the South Atlantic through the “warm route” have an average salini-
 240 ty of 35 PSU at 22°E (the Agulhas region), i.e. slightly saltier than the average salinity of
 241 NADW, which is 34.9 PSU (as quantified by the average salinity water at 6°S with densities
 242 larger than $\sigma_2 = 36.6\text{ kg/m}^3$). The upper branch of the MOC gets saltier as it flows northward,

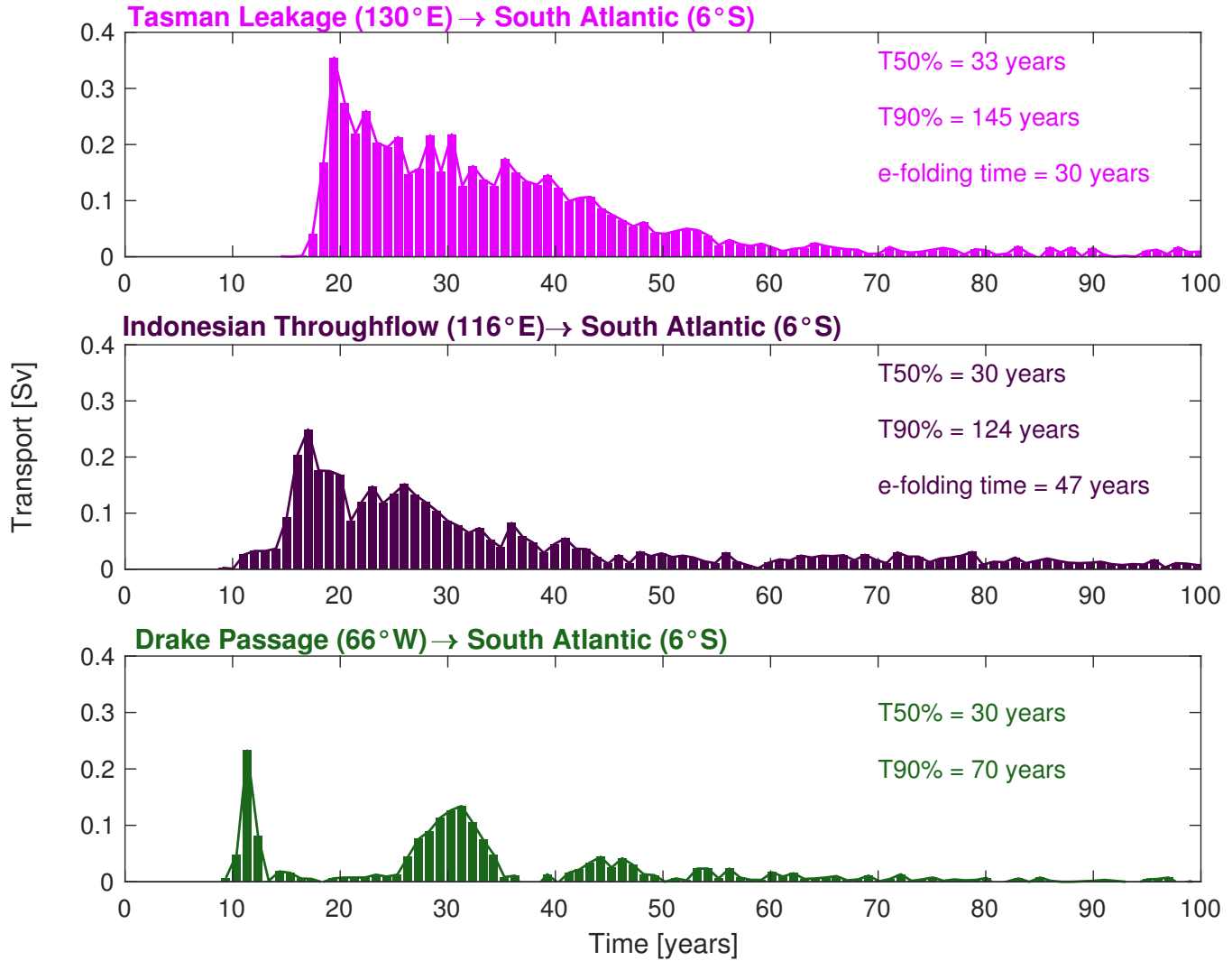


Figure 3. Distribution of transit times from the exit to each entry section weighted by transport. The inset also shows the median, the 90th percentile and the e-folding time-scales fitted to the distributions between 9 and 150 years.

243 reaching 35.6 PSU at 6°S, so that it is saltier than NADW at both 30°S and 6°S, thus export-
 244 ing freshwater out of the North Atlantic sector.

245 5 Conclusions

246 Based on a state estimate which is a close fit to most available global data constraints,
 247 we evaluate the routes and thermohaline properties of the upper branch of the MOC using a
 248 Lagrangian analysis using the three-dimensional velocities of ECCOV4. We find that the up-
 249 per branch of the MOC receives its transport primarily from the region south of Australia (Tas-
 250 man Leakage), followed by a close second contribution at the Indonesian Throughflow, and
 251 a distant third contribution from Drake Passage.

252 Eighty percent of the particle transport through 6°S originating from Drake Passage goes
 253 through the indirect cold route. This tortuous path results in a loss of identity in $\theta-S$ space.
 254 Indeed all three contributions have essentially the same properties when entering the South At-

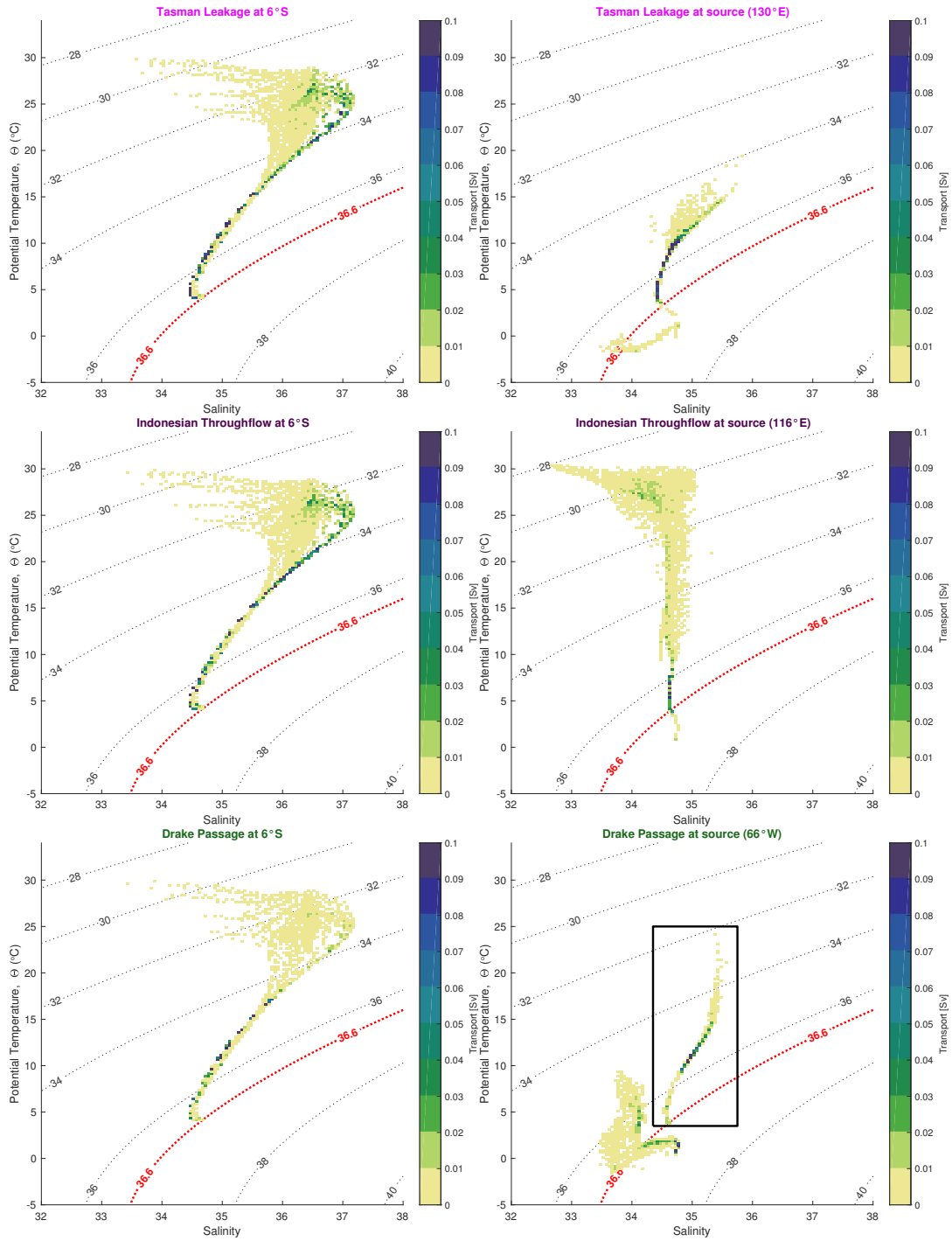


Figure 4. Particle transports binned in potential temperature/salinity space following particles at the entry (right) and exit (left) sections. Particles entering from Tasman Leakage are in the top row, from Indonesian Throughflow in the middle row, and from Drake passage in the bottom row. The boxed inset in the bottom right panel shows the θ – S relation of the particles crossing the Agulhas section at 22°E , south of Africa. This entry section carries 13.2 Sv (97% of the exit transport) compressed in a tight θ – S relation, regardless of the upstream entry point (DP, IT, or TL). The dashed lines show contours of constant σ_2 .

255 lantic, casting doubts on the ability to recognize the origin of this transport through compar-
 256 ative analysis of water masses, as remarked in Rühls et al. (2019).

257 We demonstrate that the MOC exports freshwater out of the North Atlantic sector. This
 258 is important because simple models of the MOC indicate that when the MOC exports fresh-
 259 water out of the Atlantic, the salt-advection feedback is operating, leading to potential bista-
 260 bility of the overturning circulation (Stommel, 1961; de Vries & Weber, 2005; Beal et al., 2011;
 261 Drijfhout et al., 2011).

262 Acknowledgments

263 Support by the National Science Foundation under Grant OCE-1634128 and by the National
 264 Aeronautic and Space Administration under grant 80NSSC20K0796 is gratefully acknowledged.
 265 Computational resources were provided by the Extreme Science and Engineering Discovery
 266 Environment (XSEDE) on Stampede2 at the Texas Advanced Computing Center through al-
 267 location TG-OCE130026. XSEDE is supported by the National Science Foundation grant num-
 268 ber ACI-1548562. The ECCOv4 data can be downloaded from [ftp://ecco.jpl.nasa.gov/
 269 Version4/Release3/](ftp://ecco.jpl.nasa.gov/Version4/Release3/), while the MITgcm FLT package can be downloaded from [https://
 270 github.com/MITgcm/MITgcm/tree/master/pkg/flt](https://github.com/MITgcm/MITgcm/tree/master/pkg/flt).

271 References

- 272 Beal, L. M., Ruijter, W. D., Biastoch, A., Zahn, R., Cronin, M., Hermes, J., . . . others
 273 (2011). On the role of the Agulhas system in ocean circulation and climate. *Nature*,
 274 472, 429.
- 275 Blanke, B., & Raynaud, S. (1997). Kinematics of the Pacific Equatorial Undercurrent:
 276 An Eulerian and Lagrangian approach from GCM results. *J. Phys. Oceanogr.*, 27(6),
 277 1038-1053.
- 278 Cessi, P. (2019). The Global Overturning Circulation. *Annual review of marine science*, 11,
 279 249–270.
- 280 Cessi, P., & Jones, C. (2017). Warm-route versus cold-route interbasin exchange in the
 281 meridional overturning circulation. *J. Phys. Oceanogr.*, 47, 1981–1997.
- 282 Cunningham, S., Alderson, S., King, B., & Brandon, M. (2003). Transport and variabil-
 283 ity of the Antarctic Circumpolar Current in Drake Passage. *J. Geophys. Res.: Oceans*,
 284 108(C5).
- 285 de Vries, P., & Weber, S. L. (2005). The Atlantic freshwater budget as a diagnostic for
 286 the existence of a stable shut down of the meridional overturning circulation. *Geophys.*
 287 *Res. Lett.*, 32, L09606.
- 288 Donners, J., & Drijfhout, S. (2004). The Lagrangian view of South Atlantic interocean
 289 exchange in a global ocean model compared with inverse model results. *J. Phys.*
 290 *Oceanogr.*, 34, 1019–1035.
- 291 Donohue, K., Tracey, K., Watts, D., Chidichimo, M. P., & Chereskin, T. (2016). Mean
 292 Antarctic Circumpolar Current transport measured in Drake Passage. *Geophys. Res.*
 293 *Let.*, 43, 11–760.
- 294 Döös, K. (1995). Interocean exchange of water masses. *J. Geophys. Res.*, 100, 13499–
 295 13514.
- 296 Drijfhout, S., Weber, S. L., & van der Swaluw, E. (2011). The stability of the MOC as di-
 297 agnosed from model projections for pre-industrial, present and future climates. *Clim.*
 298 *Dyn.*, 37, 1575-1586.
- 299 Forget, G., Campin, J.-M., Heimbach, P., Hill, C. N., Ponte, R. M., & Wunsch, C. (2015).
 300 ECCO version 4: an integrated framework for non-linear inverse modeling and
 301 global ocean state estimation. *Geoscientific Model Development*, 8(10), 3071–3104.
 302 Retrieved from <http://www.geosci-model-dev.net/8/3071/2015/> doi:
 303 10.5194/gmd-8-3071-2015
- 304 Forget, G., & Ferreira, D. (2019). Global ocean heat transport dominated by heat export
 305 from the tropical Pacific. *Nature Geoscience*. Retrieved from <https://doi.org/10>

- 306 .1038/s41561-019-0333-7 doi: 10.1038/s41561-019-0333-7
- 307 Forget, G., Ferreira, D., & Liang, X. (2015). On the observability of turbulent transport rates
308 by argo: supporting evidence from an inversion experiment. *Ocean Sci.*, *11*, 839-853.
- 309 Forget, G., & Ponte, R. M. (2015). The partition of regional sea level variability. *Progress in*
310 *Oceanography*, 173–195.
- 311 Fukumori, I., Wang, O., Fenty, I., Forget, G., Heimbach, P., & Ponte, R. M. (2017). *Ecco*
312 *version 4 release 3* (Tech. Rep.).
- 313 Gent, P., & McWilliams, J. C. (1990). Isopycnal mixing in ocean circulation models. *J. Phys.*
314 *Oceanogr.*, *20*, 150-155. doi: 10.1175/1520-0485(1990)020<0150:IMIOCM>2.0.CO;
315 2
- 316 Gordon, A. L. (1986). Interocean exchange of thermocline water. *J. Geophys. Res.*, *91*,
317 5037-5046.
- 318 Gordon, A. L., Weiss, R. F., Smethie, W. M., & Warner, M. J. (1992). Thermocline and in-
319 termediate water communication between the south atlantic and indian oceans. *J. Geo-*
320 *phys. Res.*, *97*, 7223–7240.
- 321 Griffies, S. M. (1998). The Gent-McWilliams skew flux. *J. Phys. Oceanogr.*, *28*(5), 831-
322 841.
- 323 Holfort, J., & Siedler, G. (2001). The meridional oceanic transports of heat and nutrients in
324 the South Atlantic. *J. of Phys. Oceanogr.*, *31*, 5–29.
- 325 Hsiung, J. (1985). Estimates of global oceanic meridional heat transport. *J. Phys. Oceanogr.*,
326 *15*, 1405-1413.
- 327 Jackson, L. C., Dubois, C., Forget, G., Haines, K., Harrison, M., Iovino, D., ... Zuo, H.
328 (2019). The mean state and variability of the north atlantic circulation: A perspec-
329 tive from ocean reanalyses. *J. Geophys. Res.: Oceans*, *124*(12), 9141-9170. doi:
330 10.1029/2019JC015210
- 331 Kang, S. M., Held, I. M., Frierson, D. M. W., & Zhao, M. (2008). The response of the ITCZ
332 to extratropical thermal forcing: Idealized slab-ocean experiments with a GCM. *J. Cli-*
333 *mate*, *21*, 3521-3532.
- 334 Macdonald, A. M. (1998). The global ocean circulation: A hydrographic estimate and re-
335 gional analysis. *Progress in Oceanography*, *41*(3), 281–382.
- 336 Redi, M. H. (1982). Oceanic isopycnal mixing by coordinate rotation. *J. Phys. Oceanogr.*,
337 *12*, 1154-1158. doi: 10.1175/1520-0485(1982)012<1154:OIMBCR>2.0.CO;2
- 338 Rintoul, S. R. (1991). South Atlantic interbasin exchange. *J. Geophys. Res.*, *96*, 2675-2692.
- 339 Rodrigues, R. R., Wimbush, M., Watts, D. R., Rothstein, L. M., & Ollitrault, M. (2010).
340 South Atlantic mass transports obtained from subsurface float and hydrographic data.
341 *J. of Mar. Res.*, *68*, 819–850.
- 342 Rühs, S., Schwarzkopf, F. U., Speich, S., & Biastoch, A. (2019). Cold vs. warm water route
343 – sources for the upper limb of the atlantic meridional overturning circulation revisited
344 in a high-resolution ocean model. *Ocean Science*, *15*(3), 489–512. Retrieved from
345 <https://www.ocean-sci.net/15/489/2019/> doi: 10.5194/os-15-489-2019
- 346 Schmitz Jr, W. J. (1995). On the interbasin-scale thermohaline circulation. *Reviews of Geo-*
347 *physics*, *33*(2), 151–173.
- 348 Sloyan, B. M., & Rintoul, S. R. (2001). Circulation, renewal, and modification of Antarctic
349 Mode and Intermediate Water. *J. Phys. Oceanogr.*, *31*(4), 1005-1030.
- 350 Speich, S., Blanke, B., & Cai, W. (2007). Atlantic meridional overturning circulation and the
351 southern hemisphere supergyre. *Geophys. Res. Lett.*, *34*, L23614. doi: doi:10.1029/
352 2007GL031583
- 353 Speich, S., Blanke, B., de Vries, P., Drijfhout, S., Döös, K., Ganachaud, A., & Marsh, R.
354 (2002). Tasman leakage: A new route in the global ocean conveyor belt. *Geophys.*
355 *Res. Lett.*, *29*(10), 55-1–55-4.
- 356 Speich, S., Blanke, B., & Madec, G. (2001). Warm and cold water routes of an ogcm ther-
357 mohaline conveyor belt. *Geophys. Res. Lett.*, *28*, 311–314.
- 358 Stommel, H. (1961). Thermohaline convection with two stable regimes of flow. *Tellus*, *13*,
359 224-230.

- 360 Talley, L. D. (2013). Closure of the global overturning circulation through the Indian, Pa-
361 cific, and Southern Oceans: Schematics and transports. *Oceanography*, 26(1), 80-97.
362 doi: 10.5670/oceanog.2013.07
- 363 Uotila, P., Goosse, H., Haines, K., Chevallier, M., Barthélemy, A., Bricaud, C., . . . others
364 (2019). An assessment of ten ocean reanalyses in the polar regions. *Clim. Dyn.*, 52,
365 1613–1650.
- 366 Young, W. R. (2012). An exact thickness-weighted average formulation of the Boussinesq
367 equations. *J. Phys. Oceanogr.*, 42(5), 692-707.

Supporting Information for "A state estimate of the routes of the upper branch of the Atlantic Meridional Overturning Circulation"

Louise Rousselet¹, Paola Cessi¹ *, Gael Forget²

¹Scripps Institution of Oceanography, University of California, San Diego, USA

²Dept. of Earth, Atmospheric and Planetary Sciences, Massachusetts Institute of Technology, Cambridge, MA, USA

Contents of this file

1. Text S1 to S4
2. Figure S1

Additional Supporting Information (Files uploaded separately)

1. Captions for Movies S1 to S2

*Paola Cessi, Scripps Institution of
Oceanography,
University of California, San Diego,
La Jolla, CA 92039-0213, USA

Introduction

A description of the algorithm and software used for the Lagrangian trajectories is provided, together with two animations of four typical particle trajectories.

Particle-trajectory calculation

ECCOv4 provides the three-dimensional velocity field on a gridded mesh in latitude, longitude and depth for the 24 years of the assimilated period. We use the monthly climatological average repeated for 2011 years over the annual period. In order to preserve the conservation properties of the gridded ECCOv4 fields, and in particular the incompressibility of the velocity, it is important to use the fields on the native curvilinear grid. The global domain of ECCOv4 is decomposed in 13 tiles, and particle trajectories must be exchanged across the tiles' boundaries (Forget et al., 2015). To our knowledge, the only code that is capable of seamlessly exchanging particles across tiles on the three dimensional ECCOv4 curvilinear grid is the FLT package within the MITgcm suite and this is what we used (Campin et al., 2019). Additionally, the FLT package is computationally efficient on the multi-processor, multi-node supercomputer available to us.

The spatial interpolation algorithm for the velocity field was modified according to Döös (1995), to *linearly* interpolate the *transport* associated with each velocity component on the staggered grid used by ECCOv4: in this way incompressibility of the velocity is guaranteed at every point along the particle trajectory. With velocity incompressibility satisfied exactly, particles never reach the land points where the velocity vanishes. Unlike Döös (1995), we use a 4th order Runge-Kutta scheme to time-step the trajectories; this introduces a small error in the time-integration, without violating incompressibility.

Particle-trajectory animations

In figure S1 and in the associated animations, four particles are tracked from their initial entry in one of the sections to the exit section at 6°S in the Atlantic. The particles are chosen as they best represent: (i) the average temperature and salinity at each entry section (i.e. ± 0.2 from mean T°C and ± 0.1 PSU from mean salinity); (ii) the median transit times shown in Figure 2 (i.e. ± 15 years from T50%). Particle entering through Tasman Leakage and Indonesian Throughflow are shown respectively with a diamond and a circle. Both "direct" and "indirect" cold routes from Drake Passage are shown by two different trajectories (stars). In addition to the position, which is shown every 3 months, the color of the particle denotes its temperature or salinity at that position, allowing to visualize the thermodynamic transformations occurring along each trajectory. The temperature and salinity variations over time (along trajectories) are also displayed in the bottom right inset. The bottom left legend indicates the arrival time of each particle at 6°S.

Movie S1. Positions of four particles along typical trajectories from the entry sections are shown every 3 months with different symbols: stars denote particles entering at DP, diamonds are for entry at TL, and dots are for entry at IT. The color of the symbols denotes salinity (in PSU). The salinity evolution for each particle is shown in the bottom right inset. The bottom left legend indicates the arrival time of each particle at 6°S.

Movie S2. Positions of four particles along typical trajectories from the entry sections are shown every 3 months with different symbols: stars denote particles entering at DP, diamonds are for entry at TL, and dots are for entry at IT. The color of the symbols

denotes potential temperature (in ° C). The temperature evolution for each particle is shown in the bottom right inset. The bottom left legend indicates the arrival time of each particle at 6°S.

References

- Campin, J.-M., Heimbach, P., Losch, M., Forget, G., edhill3, Adcroft, A., ... McRae, A. T. T. (2019, October). *Mitgcm/mitgcm: checkpoint67m*. Zenodo. Retrieved from <https://doi.org/10.5281/zenodo.3492298> doi: 10.5281/zenodo.3492298
- Döös, K. (1995). Interocean exchange of water masses. *J. Geophys. Res.*, *100*, 13499–13514.
- Forget, G., Campin, J.-M., Heimbach, P., Hill, C. N., Ponte, R. M., & Wunsch, C. (2015). ECCO version 4: an integrated framework for non-linear inverse modeling and global ocean state estimation. *Geoscientific Model Development*, *8*(10), 3071–3104. Retrieved from <http://www.geosci-model-dev.net/8/3071/2015/> doi: 10.5194/gmd-8-3071-2015

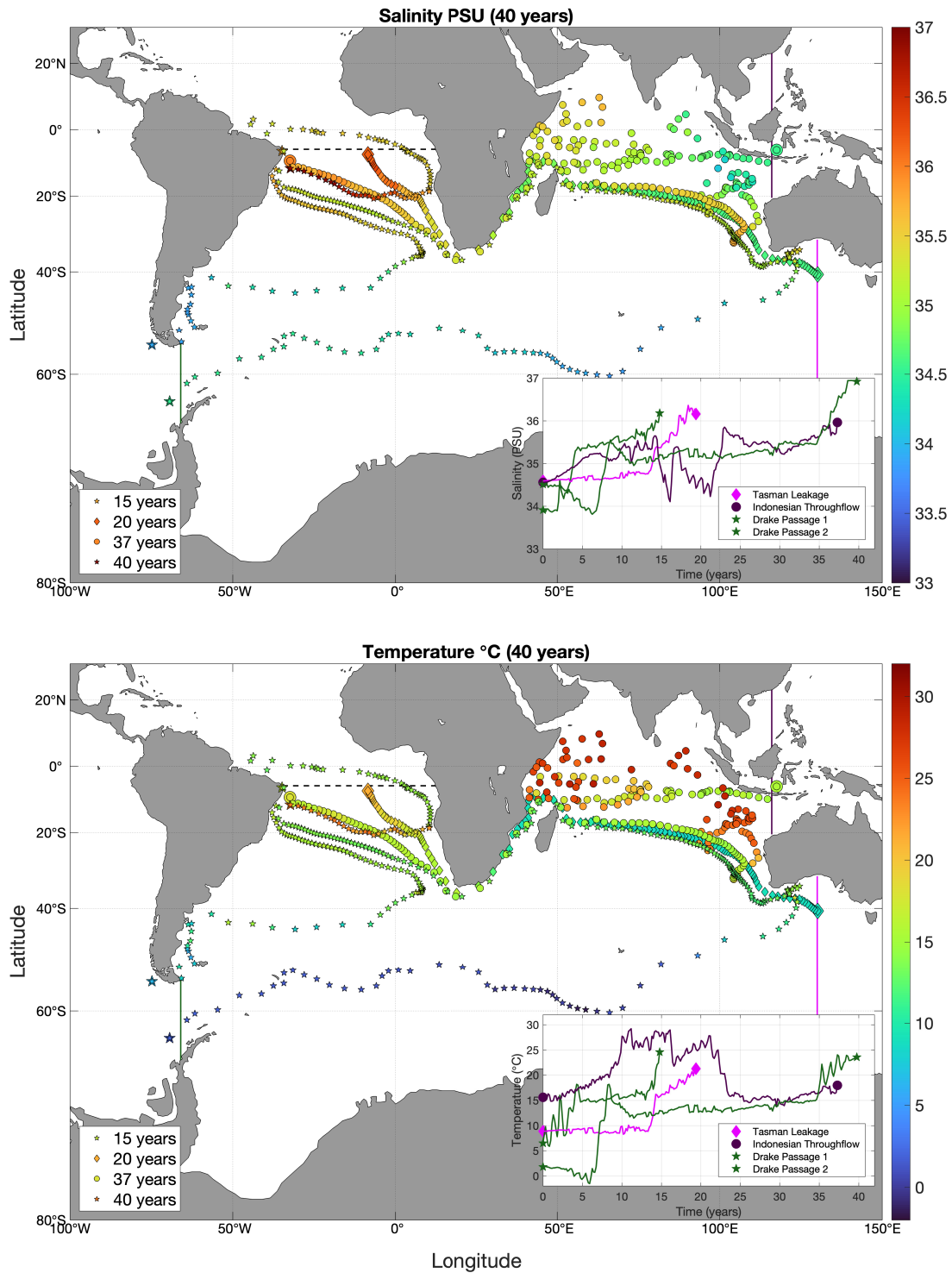


Figure S1. Positions of four particles along typical trajectories from the entry sections are shown every 3 months with different symbols: stars denote particles entering at DP, diamonds are for entry at TL, and dots are for entry at IT. The color or the symbols denote salinity (in PSU) in the top panel and potential temperature in the bottom panel (in ° C). The salinity and temperature evolution for each particle is shown in the bottom right inset. The bottom left legend indicates the arrival time of each particle at 6°S.